

# Mixed Convection in Superposed Nanofluid and Porous Layers Inside Lid-Driven Square Cavity

Ahlam A. Hassan, Muneer A. Ismael\*

Mechanical Engineering Department, Engineering College, University of Basrah, Basrah 61004, Iraq.

## Abstract

Mixed convection in a lid-driven composite square cavity is studied numerically. The cavity is composed of two layers; a Cu–water nanofluid layer superposed a porous layer. The porous layer is saturated with the same nanofluid. The left and right walls of the cavity are thermally insulated. The bottom wall which is in contact with the porous layer is isothermally heated and being lid to the left, while the top wall is isothermally cooled and being lid to the right. Cavity walls are impermeable except the interface between the porous layer and the nanofluid. Maxwell-Brinkman model is invoked for the momentum exchange within the porous layer. Equations govern the conservation of mass, momentum, and energy within the two layers were modeled and solved numerically using under successive relaxation (USR) up-wind finite difference scheme. Four pertinent parameters are studied; nanoparticles volume fraction  $\phi$  (0.0 - 0.05), porous layer thickness  $W_p$  (0.1 - 0.9), Darcy number  $Da$  ( $10^{-7} - 10^{-1}$ ), and Richardson number  $Ri$  (0.01 - 10). The results have showed that the existence of the porous layer in a specified value can enhance the convective heat transfer when  $Ri \geq 1$ , while an adverse action of nanoparticles is recorded when  $Da = 10^{-4}$ .

**Keywords:** Composite cavity; lid-driven; porous medium; nanofluid.

## 1. Introduction

Mixed convection flow and heat transfer in enclosures are encountered in a number of industrial applications such as, float glass manufacturing, during solidification of ingots, coating or continuous reheating furnaces, and any application possesses a solid material motion inside a chamber. The mixed convection flow in lid-driven cavity or enclosure is generated from two mechanisms. The first is due to shear flow caused by the movement of one (or two) of the cavity wall while the second is due to the buoyancy flow induced by the non homogeneous thermal boundaries. This type of heat transfer is complex because of coupling between shear force caused by movement of wall and the buoyancy force by temperature difference on the boundary of domain. Cavity flow simulation was introduced in early studies (Torrance et al. [1] and Ghia et al. [2]). During those days, performance of a computer to do simulations was not as accurate as it is nowadays. As the performance of the technology of hardware as well as software improves, simulation has

become a simple task. Lid-driven cavities are found studied in various situations such as pure or nanofluid filled cavities, and pure or nanofluid saturated porous medium cavities. Lid-driven cavities filled with pure fluids as in Koseff [3], Mohamad and Viskanta [4], Mekrouss et al. [5], Sivasankaran et al. [6], or in nanofluid filled cavities as in Tiwari and Das [7], Talebi et al. [8], Abu-Nada and Chamkha [9], Chamkha and Abu Nada [10], Abbasian et al. [11], Chang Cho et al. [12]. Lid-driven pure fluid filled cavities as in Oztop et al. [13], Muthamilselvan et al. [14]. Lid-driven nanofluid saturated porous cavities as in Sun and Pop [15], Chamkha and Ismael [16], Bourantas et al. [17], Yasin et al. [18].

Industrially and environmentally, the natural convection heat transfer in a composite cavity layered by fluid and porous media, vertically or horizontally matched, is widely encountered in: packed bed solar energy storage, directional solidification of binary alloys, fibrous and granular insulation systems, thermal circulation in lakes and shallow coastal areas, and contaminant transport in groundwater. The porous layer superimposed by a fluid layer can be found in the following studies: Chen & Chen [19] who performed a nonlinear computational investigation of thermal convection due to

\*Corresponding author. Tel.: +9647801043835

Fax: +9647801043835; E-mail: muneerismael@yahoo.com

© 2015 International Association for Sharing Knowledge and Sustainability

DOI: 10.5383/ijtee.10.02.002

heating from below in a porous layer underlying a fluid layer. The motion of the fluid in the porous layer is governed by Darcy's equation with the Brinkman terms for viscous effects and the Forchheimer term for inertial effects included. Goyeau et al. [20] conducted a study deals with natural convection driven by combined thermal and solutes buoyancy forces in a binary fluid. Their configuration is a confined enclosure partially filled with a vertical porous layer. Their mathematical description of the problem is based on the one-domain formulation of the conservation equations. Their numerical results showed quantitatively the influence of the porous layer on the flow structure and on heat and species transfer in the enclosure. Baytas et al. [21] investigated the double diffusive natural convection between a saturated porous layer and an overlying fluid layer in an enclosure using the non-Darcy flow model. The problem has been investigated for two cases; namely case I where the interface between fluid and porous layer is horizontal, and case II where the interface contains a step with different heights. The fluid flow and heat and mass transfer has been investigated for different values of the step height and the Rayleigh and Darcy numbers. The results showed that the height of the step at the interface has a significant effect on the flow field and heat and mass transfer. Bagchi and Kulacki [22] studied numerically the natural convection in fluid–superposed porous layers heated locally from below based on the one-domain formulation of the conservation equations. They reported that Nusselt numbers increase with a decrease in the heater length and height ratio, and increase with the Darcy number. Their results represent an extension of the well studied problem of buoyant convection in fluid–superposed porous layers with a fully heated lower surface. Bagchi and Kulacki [23] conducted an experimental study of natural convection in fluid–superposed porous layers heated locally from below. Measurements are made in a rectangular chamber with 3 mm diameter glass beads as the porous layer and distilled water as the saturating fluid. The effects of the heater-to-cavity length ratio and the porous layer-to-cavity height ratio on the overall heat transfer coefficients are reported. Average heat transfer coefficients over the heated surface increase with a decrease in porous layer-to-cavity height ratio, but no clear effect of heater-to-cavity length ratio is seen. Temperature profiles in the domain reveal a plume like flow with a single pair of circulating cells and evidence of convective motion inside the porous layer. Chamkha and Ismael [24] studied numerically the laminar natural convection inside rectangular composite vertically-layered cavities. The porous layer is saturated with the same nanofluid. Double–domain formulation is followed for the porous and nanofluid layers with alternative models for the nanofluid thermal conductivity and dynamic viscosity. Their results showed that with aid of nanofluid the enhancement of natural convection can be attained even for low permeability porous medium. They reported also a critical thickness for the porous layer at which the convective heat transfer is maximum. However, the critical literature survey regarding the topics above, led to ascertain that the mixed convection in a composite layered cavity filled with nanofluid has not been investigated before. This motivates us to consider a square cavity composed of a horizontal nanofluid superposed a porous layer heated from below and subjected to shear effect via counter movement of the horizontal walls. It is thought that this study will enhance the corroboration of the knowledge in the contributions of nanofluid and porous media in heat transfer within many engineering and geophysical applications

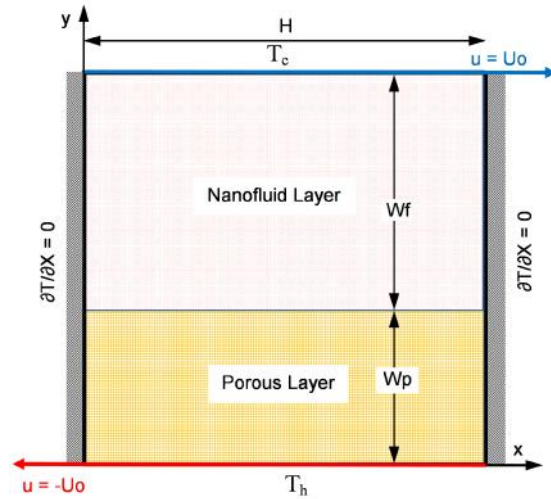


Fig. 1 Physical domain and coordinates system

## 2. Mathematical Modeling

The considered problem is shown schematically in Fig. 1. It is a square cavity with  $H$  side long. A horizontal porous layer of thickness  $W_p$  is localized on the bottom part of the cavity and saturated with a nanofluid. This nanofluid fills the remainder of the cavity ( $H - W_p$ ). The bottom wall of the cavity which is in contact with the porous layer is heated isothermally, and kept at  $T_h$ , while the top wall of the cavity is cooled isothermally, and kept at  $T_c$ . Mathematically, there exist two approaches for dealing with porous–nanofluid layer cavity, namely, the single–domain approach and the double domain approach. The former put one set of governing equations for both layers with a binary parameter that modifies the momentum equation to applicable in any layer. It is simple and requires less boundary condition. But it restricted by formulating the grid in such manner that no grids located along the interface. On the other hand, the double–domain approach employs a separated set of equations for each layer. The two sets are matched by appropriate boundary conditions along the interface. In the present study, and to avoid the restriction of the grid localization due to the interface, the double–domain approach is to be used. Darcy–Brinkman model is invoked to represents the convection within the porous layer, where in this model there is no problem in the order of the matched momentum equation in the nanofluid and porous layers. The following assumptions are used to simplify the proposed model: The flow is two-dimensional, incompressible, laminar, and steady state. All outer boundaries are impermeable, while the horizontal interface between nanofluid and porous layers is permeable. Regarding the porous layer, uniform and undeformable pores between the solid matrixes. They (the base fluid and the nanoparticles) are in thermal equilibrium and no slip occur between them. A thermal equilibrium between the nanofluid filling pores and the solid matrix. Mixed convection flow is a steady, laminar, and with constant physical properties except the density where it varies with temperature according to Boussinesq approximation. The energy dissipation and radiation of surface are negligible. The Navier–Stokes equation based on the previous assumptions in Cartesian coordinates for (porous and nanofluid layers) can be written as follow:

For the porous layer:

Continuity:

$$\frac{\partial u_p}{\partial x} + \frac{\partial v_p}{\partial y} = 0 \quad (1)$$

x-direction momentum equation:

$$\rho_{nf} \left( u_p \frac{\partial u_p}{\partial x} + v_p \frac{\partial u_p}{\partial y} \right) = -\varepsilon^2 \frac{\partial p}{\partial x} + \varepsilon \mu_{nf} \left( \frac{\partial^2 u_p}{\partial x^2} + \frac{\partial^2 u_p}{\partial y^2} \right) - \varepsilon^2 \frac{\mu_{nf}}{K} u_p \quad (2)$$

y-direction momentum equation:

$$\rho_{nf} \left( u_p \frac{\partial v_p}{\partial x} + v_p \frac{\partial v_p}{\partial y} \right) = -\varepsilon^2 \frac{\partial p}{\partial y} + \varepsilon \mu_{nf} \left( \frac{\partial^2 v_p}{\partial x^2} + \frac{\partial^2 v_p}{\partial y^2} \right) - \varepsilon^2 \frac{\mu_{nf}}{K} v_p + \varepsilon^2 \rho_{nf} \beta_{nf} g (T_p - T_c) \quad (3)$$

Energy equation:

$$u_p \frac{\partial T_p}{\partial x} + v_p \frac{\partial T_p}{\partial y} = \alpha_{eff} \left( \frac{\partial^2 T_p}{\partial x^2} + \frac{\partial^2 T_p}{\partial y^2} \right) \quad (4)$$

For nanofluid layer:

Continuity:

$$\frac{\partial u_{nf}}{\partial x} + \frac{\partial v_{nf}}{\partial y} = 0 \quad (5)$$

X-direction momentum equation:

$$\rho_{nf} \left( u_{nf} \frac{\partial u_{nf}}{\partial x} + v_{nf} \frac{\partial u_{nf}}{\partial y} \right) = -\frac{\partial p}{\partial x} + \mu_{nf} \left( \frac{\partial^2 u_{nf}}{\partial x^2} + \frac{\partial^2 u_{nf}}{\partial y^2} \right) \quad (6)$$

Y-direction momentum equation:

$$\rho_{nf} \left( u_{nf} \frac{\partial v_{nf}}{\partial x} + v_{nf} \frac{\partial v_{nf}}{\partial y} \right) = -\frac{\partial p}{\partial y} + \mu_{nf} \left( \frac{\partial^2 v_{nf}}{\partial x^2} + \frac{\partial^2 v_{nf}}{\partial y^2} \right) + \rho_{nf} \beta_{nf} g (T_{nf} - T_c) \quad (7)$$

Energy equation:

$$u_{nf} \frac{\partial T_{nf}}{\partial x} + v_{nf} \frac{\partial T_{nf}}{\partial y} = \alpha_{nf} \left( \frac{\partial^2 T_{nf}}{\partial x^2} + \frac{\partial^2 T_{nf}}{\partial y^2} \right) \quad (8)$$

Where  $\phi$  is the porosity of the porous medium,  $\beta$  is the thermal expansion coefficient,  $\rho$  is the density,  $K$  is the permeability of the porous medium,  $\mu$  is the dynamic viscosity, and  $\alpha$  is the thermal diffusivity. The subscripts p and nf stand for porous and nanofluid, respectively.

For the given problem, the appropriate boundary conditions at the system boundaries are,

1- At  $y = 0$  (bottom wall),  $u = -U_o$ ,  $v = 0$   $T = T_h$

2- At  $y = H$  (top wall),  $u = U_o$ ,  $v = 0$   $T = T_c$

3- At  $x = 0$  (left wall) and  $x = H$  (right wall),  $u = v = 0$ ,  $\frac{\partial T}{\partial x} = 0$

4- At  $y = W_p$  (interface):

$$u_p = u_{nf}, \quad v_p = v_{nf}$$

$$\tau_p = \tau_{nf}, \quad \mu_{eff} \left( \frac{\partial u}{\partial y} + \frac{\partial v}{\partial x} \right)_p = \mu_{nf} \left( \frac{\partial u}{\partial y} + \frac{\partial v}{\partial x} \right)_{nf}$$

$$T_p = T_{nf}, \quad -k_{eff} \frac{\partial T_p}{\partial y} = -k_{nf} \frac{\partial T_{nf}}{\partial y}$$

where  $\tau$  is the shear stress.

In the present study the considered base fluid and the nanoparticles are water and Copper Cu, respectively with thermo-physical properties shown in Table 1 [24]. The adopted relations that prescribe the physical properties of the nanofluid depend only on the nanoparticles volume fraction  $\phi$  and what are proven and used in many studies and as follow:

**Table 1: Thermo physical properties of fluid and nanoparticles [24]**

Physical property	Base fluid (water)	Nanoparticle (Cu)
Cp (J/kg K)	4179	385
(kg/m <sup>3</sup> )	997.1	8933
k (W/m.K)	0.613	400
x 10 <sup>-5</sup> (1/K)	21	1.67

$$\rho_{nf} = (1 - \phi)\rho_f + \phi\rho_{np} \quad (9)$$

$$\beta_{nf} = (1 - \phi)\beta_f + \phi\beta_{np} \quad (10)$$

Thermal diffusivity:

$$\alpha_{nf} = \frac{k_{nf}}{(\rho Cp)_{nf}} \quad (11)$$

$$\alpha_{eff} = \frac{k_{eff}}{(\rho Cp)_{nf}} \quad (12)$$

$$k_{eff} = (1 - \varepsilon)k_s + \varepsilon k_{nf} \quad (13)$$

Where  $k_s$  is the thermal conductivity of the solid matrix forming the porous layer.

Heat capacity:

$$(\rho Cp)_{nf} = (1 - \phi)(\rho Cp)_f + \phi(\rho Cp)_{np} \quad (14)$$

Thermal conductivity, based on Maxwell-Garnetts (MG):

$$k_{nf} = \frac{(k_{np} + 2k_f) - 2\phi(k_f - k_{np})}{(k_{np} + 2k_f) + \phi(k_f - k_{np})} k_f \quad (15)$$

Viscosity based on Brinkman model [25]:

$$\mu_{nf} = \frac{\mu_f}{(1 - \phi)^{2.5}} \quad (16)$$

Although there exists many modified models for the thermal conductivity and dynamic viscosity of nanofluids, the MG and Brinkman models still give reasonable results but for low volume fractions of nanoparticles, Khanafar and Vafai [26].

The formulation is based on the stream function,  $u = \frac{\partial \psi}{\partial y}$ ,  $v = -\frac{\partial \psi}{\partial x}$  and the vorticity,  $\omega = \frac{\partial v}{\partial x} - \frac{\partial u}{\partial y}$ , and on the following non-

dimensional parameters  $X = \frac{x}{H}$ ,  $Y = \frac{y}{H}$ ,  $W_p = \frac{w_p}{H}$ ,  $U = \frac{u}{U_o}$ ,  $V = \frac{v}{U_o}$ ,  $\Psi = \frac{\psi}{HU_o}$ ,  $\omega = \frac{\omega H}{U_o}$ ,  $\theta = \frac{T - T_c}{T_h - T_c}$ . Following the usual manipulation of eliminating pressure gradient terms from momentum equations, the dimensionless governing Equations become:

For porous layer

Continuity:

$$\frac{\partial^2 \Psi_p}{\partial X^2} + \frac{\partial^2 \Psi_p}{\partial Y^2} = -\Omega_p \quad (17)$$

Momentum:

$$\frac{\partial \Psi_p}{\partial Y} \frac{\partial \Omega_p}{\partial X} - \frac{\partial \Psi_p}{\partial X} \frac{\partial \Omega_p}{\partial Y} = \varepsilon \frac{v_{nf}}{v_f} \frac{1}{Re} \left[ \frac{\partial^2 \Omega_p}{\partial X^2} + \frac{\partial^2 \Omega_p}{\partial Y^2} \right] - \varepsilon^2 \frac{v_{nf}}{v_f} \frac{1}{Re Da} \Omega_p + \frac{\beta_{nf}}{\beta_f} \varepsilon^2 Ri \frac{\partial \theta}{\partial X} \quad (18)$$

Energy:  

$$\frac{\partial \Psi_p}{\partial Y} \frac{\partial \theta_p}{\partial X} - \frac{\partial \Psi_p}{\partial X} \frac{\partial \theta_p}{\partial Y} = \frac{\alpha_{nf}}{\alpha_f} \frac{1}{Pr Re} \left[ \frac{\partial^2 \theta_p}{\partial X^2} + \frac{\partial^2 \theta_p}{\partial Y^2} \right] \quad (19)$$

and for nanofluid:

Continuity:  

$$\frac{\partial^2 \Psi_{nf}}{\partial X^2} + \frac{\partial^2 \Psi_{nf}}{\partial Y^2} = -n_f \quad (20)$$

Momentum  

$$\frac{\partial \Psi_{nf}}{\partial Y} \frac{\partial \Omega_{nf}}{\partial X} - \frac{\partial \Psi_{nf}}{\partial X} \frac{\partial \Omega_{nf}}{\partial Y} = \frac{v_{nf}}{v_f} \frac{1}{Re} \left[ \frac{\partial^2 \Omega_{nf}}{\partial X^2} + \frac{\partial^2 \Omega_{nf}}{\partial Y^2} \right] + \frac{\beta_{nf}}{\beta_f} Ri \frac{\partial \theta_{nf}}{\partial X} \quad (21)$$

Energy:  

$$\frac{\partial \Psi_{nf}}{\partial Y} \frac{\partial \theta_{nf}}{\partial X} - \frac{\partial \Psi_{nf}}{\partial X} \frac{\partial \theta_{nf}}{\partial Y} = \frac{\alpha_{nf}}{\alpha_f} \frac{1}{Pr Re} \left[ \frac{\partial^2 \theta_{nf}}{\partial X^2} + \frac{\partial^2 \theta_{nf}}{\partial Y^2} \right] \quad (22)$$

where  $Pr = \frac{\nu_f}{\alpha_f}$  is the Prandtl number,  $Gr = \frac{g\beta_f \Delta T H^3}{\nu_f^2}$  is the

Grashof number,  $Da = \frac{K}{H^2}$  is the Darcy number, and  $Ri = \frac{Gr}{Re^2}$  is the Richardson number.

The dimensionless conditions on the outer boundaries of the cavity become;

$$\begin{aligned} \frac{\partial \Psi}{\partial Y} &= -1, \quad = 1, \quad = -\left(\frac{\partial^2 \Psi}{\partial Y^2}\right) \text{ at } Y=0 \\ \frac{\partial \Psi}{\partial Y} &= 1, \quad = 0, \quad = -\left(\frac{\partial^2 \Psi}{\partial Y^2}\right) \text{ at } Y=1 \\ \frac{\partial \Psi}{\partial Y} &= 0, \quad / Y=0, \quad = -\left(\frac{\partial^2 \Psi}{\partial X^2}\right) \text{ at } X=0, H \end{aligned}$$

The interface boundary conditions are derived from equating (continuity) of tangential and normal velocities, shear stress, temperature and the heat flux across the interface, and assuming the same dynamic viscosity ( $\mu_{eff} = \mu_{nf}$ ) in both layers. The agreement of this assumption was proved experimentally by Neale and Nader [27] and adopted by Sheremet and Trifonova [28]. Hence, the interface conditions can be written as;

$$\theta_p = \theta_{nf}, \quad \frac{\partial \theta_{nf}}{\partial Y} = \frac{k_{eff}}{k_{nf}} \frac{\partial \theta_p}{\partial Y} \quad (23 a)$$

$$\Psi_p = \Psi_{nf}, \quad \frac{\partial \Psi_{nf}}{\partial Y} = \frac{\partial \Psi_p}{\partial Y} \quad (23 b)$$

$$P = n_f \quad \frac{\partial \Omega_{nf}}{\partial Y} = \frac{\partial \Omega_p}{\partial Y} \quad (23 c)$$

The local Nusselt number is defined as follows:

$$Nu_{loc} = -\frac{k_{eff}}{k_f} \frac{\partial \theta}{\partial Y}$$

The average Nusselt number along the bottom wall is:

$$Nu_{av} = \frac{1}{H} \int_0^H Nu_{loc} dx \quad (24)$$

### 3. Numerical Solution and Validations

The square domain was discretized into  $N_x \times N_y$  grids. The governing equations (17 – 22) were solved numerically using the central finite difference method. Gauss-Seidel iteration procedure with Successive Under Relaxation (SUR) method is followed in the solution. The convective terms of the

momentum and energy equations were treated by the up-wind scheme to attain the solution stability. The stream function, vorticity, and dimensionless temperature are to be calculated from continuity, momentum, and energy equations, respectively. Along the solid boundaries, the condition on was interpreted using Wilkes formula [29] as;

$$\Omega_{o,j} = \frac{8\Psi_{o+1,j} - \Psi_{o+2,j}}{2\Delta n^2} - \delta \frac{3}{\Delta n} \quad (25)$$

$$\text{where } \delta = \begin{cases} 1 & \text{for moving boundary} \\ 0 & \text{for fixed boundary} \end{cases}$$

Where  $o$  represents the boundary node and  $n$  is the interval normal to this boundary. The conditions on the nanofluid–porous layers and on interfaces (equations (23 a–c)) are interpreted numerically by taking three points backward gradient and three points forward gradient at each interface. Accordingly, the following differences equations are invoked to compute the interface potentials;

$$\theta_i(i,j) = \frac{4\theta_{nf}(i,j+1) - \theta_{nf}(i,j+2) + 4Kr\theta_p(i,j-1) - Kr\theta_p(i,j-2)}{3(1+Kr)} \quad (26 a)$$

$$\Psi_i(i,j) = \frac{4\Psi_{nf}(i,j+1) - \Psi_{nf}(i,j+2) + 4\Psi_p(i,j-1) - \Psi_p(i,j-2)}{6} \quad (26 b)$$

$$i_i(i,j) = \frac{4\Omega_{nf}(i,j+1) - \Omega_{nf}(i,j+2) + 4\Omega_p(i,j-1) - \Omega_p(i,j-2)}{6} \quad (26 c)$$

Where the subscripts  $i$  refers to the interface between the porous–nanofluid layers, and  $K_r = \frac{k_{eff}}{k_{nf}}$  is the ratio of the effective thermal conductivity of the porous layer (Eq. (12)) to the thermal conductivity of the nanofluid (Eq. (15))

The convergence of the numerical solution is determined when the following criterion is satisfied.

$$\max \left| \left[ \frac{\chi_{new}(i,j) - \chi_{old}(i,j)}{\chi_{old}(i,j)} \right] \right| \leq 10^{-6} \quad (27)$$

Where denotes to any variable, , , or . An extensive mesh testing procedure was conducted to guarantee a grid independent solution. In Fig. 2 various mesh combinations were explored for the case of  $Da = 10^{-6}$ ,  $Re = 100$ ,  $Ri = 10$ ,  $Pr = 6.26$ ,  $Wp = 0.5, 0.7$ , and  $\phi = 0.0, 0.01$ . The present numerical solution was tested for grid independence by calculating the average Nusselt number on both horizontal walls. In harmony with this, it was found that a grid size of  $81 \times 81$  ensures a grid independent solution. The present numerical solution was further validated by comparing the present numerical solution results for  $Gr = 100$ ,  $Pr = 6.26$ , and three other different parameters with the numerical results of Abu-Nada and chamkha [9]. Two different tests are presented, the first is the variation of average Nusselt number with the volume fraction of the nanoparticles and the second is for the horizontal (U) velocity component at mid section of the cavity (i.e.  $X = 0.5$ ). The nanoparticles used are alumina ( $Al_2O_3$ ) where the thermo-physical properties of these nanoparticles are listed in [9]. As shown in Fig. 3, the present numerical solution is in good agreement with Abu-Nada and Chamkha [9]. Moreover, the comparisons was paid further by calculating the average Nusselt number at the top (hot) wall for  $Gr = 100$ , the work of Waheed [30], i.e. pure fluid (air). The results of comparisons are presented in Table 2. Good agreement is also obtained. Hence, the numerical approximation used in the present paper is reliable.

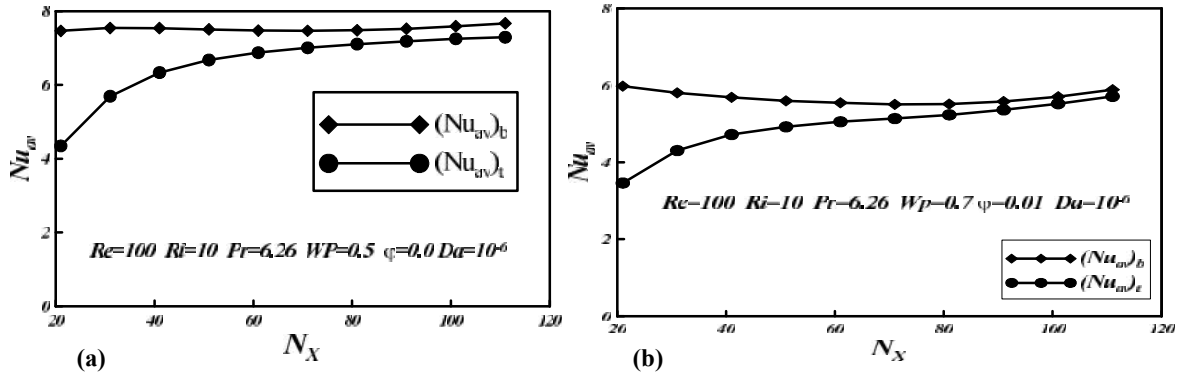


Fig. 2 Grid independency test

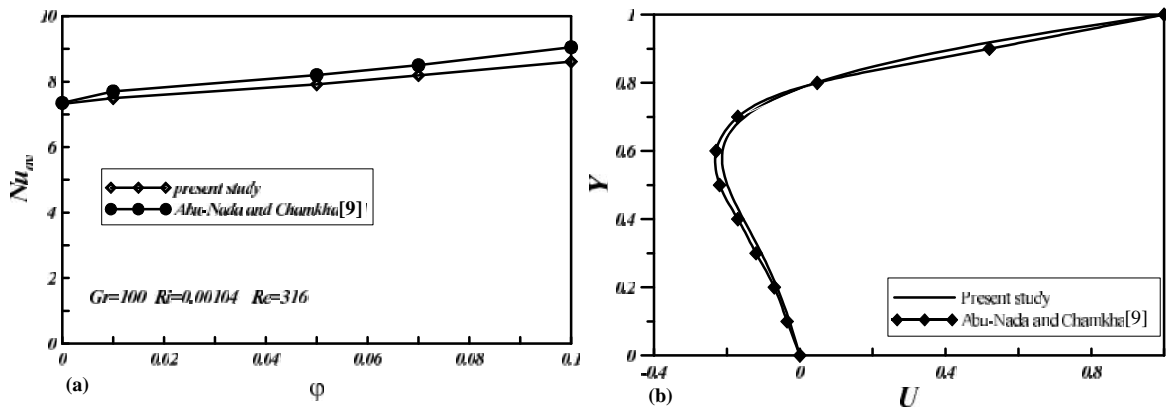


Fig. 3 Comparison of (a) average Nusselt number with nanoparticles volume fraction, and (b) horizontal velocity component along  $X = 0.5$ , for  $(Al_2O_3\text{-water})$  nanofluid cavity for  $Ri = 0.00104$  and  $Re = 316$

Table 2: Validation: Average Nusselt number over the lid surface for  $Gr = 100$

Re	Ri	Waheed [30]	Present
100	0.01	2.08405	2.03116
400	0.00062	4.047	4.02462
500	0.0004	4.5006	4.52671
1000	0.0001	5.9357	6.48423

#### 4. Results and Discussion

The results of the present work are to be illustrated graphically by contour maps of stream function (streamlines) and dimensionless temperature (isotherms), local and average Nusselt numbers. The parameters those expected to have significant effects on the convection within such composite cavity composed of nanofluid layer overlaying a saturated porous layer are: Richardson number  $Ri$  (0.01-10), Darcy number  $Da$  ( $10^{-7} - 1$ ), thickness of porous layer  $Wp$  (0.1 – 0.9) and volume fraction of the nanoparticles  $\phi$  (0.0 – 0.05). Richardson number is a comparative measure of the natural to forced convections ratio. Darcy number sometimes called dimensionless permeability of porous medium.

The value of the porous layer porosity is fixed at  $\epsilon = 0.398$  which corresponds to 3 mm diameter glass beads having a thermal conductivity of  $0.845 \text{ W/m.k}$  [23].

#### 4.1 Contour Maps

Figures 4 to 6 show typical contour maps for the streamlines and isotherms for three parameters ( $Wp$ ,  $Da$ ,  $Ri$ ). Figure 4 illustrates the effect of porous layer thickness ( $Wp = 0.1, 0.5, 0.7$ ) at 0% and 0.03% nanoparticle volume fractions for  $Ri = 1$ , and  $Da = 10^{-2}$ . The streamlines manifests the most common behavior published in many previous works, a single-eye vortex occupies most of the cavity with small perturbations at the tail of each moving wall. But in the present case, the streamlines have a steeper gradient close to the moving lower wall. The effect of the porous layer thickness can be distinguished by the reduction of the vortex strength with increasing  $Wp$ . The isotherm maps (the right column of Fig. 4) shows an isothermal zone at the middle of the cavity with noticeable thermal boundary layers close to each moving wall showing convective heat transfer. Along the vertical adiabatic walls, the isotherms are mostly vertical. It is worth mentioning to note that the dashed contours refer to the nanofluid ( $\phi = 0.03$ ) and the solid contours refer to pure fluid. Accordingly, the addition of nanoparticles can be distinguished by the isotherms more than the streamlines. This can be attributed to

that the shear action provided by the movement of the two horizontal walls is large enough to overcome the viscous and inertia forces promoted in the nanofluid. Due to this, the streamlines appear to be less effected by the nanofluid addition. This attribution can be applied for the following contours too. Figure 5 presents the effect of Darcy number for  $Ri = 1$  and  $Wp = 0.5$ . When  $Da = 10^{-1}$ , the streamlines behavior is as same as that discussed in Fig. 4. When  $Da$  is decreased, the vortex core is shifted to the upper part of the cavity and tends to follow the direction of the moving upper wall. Moreover, the streamlines are crowded close to the moving upper wall which indicates to the intensification of nanofluid flow there. Within the porous layer, the streamlines tends to plume towards the lower corners at  $Da = 10^{-4}$ . When  $Da = 10^{-7}$ , the streamlines reflects the restricted motion of the nanofluid in the porous layer. The isothermal zone which is localized at the middle of the cavity at  $Da = 10^{-1}$  is transmitted to the right upper part of the cavity with decreasing Darcy.

The effect of Richardson number is illustrated in Fig. 6 for  $Wp = 0.5$  and  $Da = 10^{-3}$ . For very low value of Richardson number ( $Ri = 0.01$ ), the lid effect (forced convection) is dominated over the natural convection. Therefore, double-eye vortex is generated in this case where the nanofluid movement is mainly due to the shear effect provided by the moving walls. When  $Ri$  is increased to unity (equivalent convection modes), the natural convection starts to affect the nanofluid motion by increasing its strength. When  $Ri$  is further increased to 10, the natural convection becomes the dominant mode and this leads to strengthen the streamlines and form it in a strong single-eye vortex rotates freely in the nanofluid layer. The isotherm maps contours (the right column of Fig. 6) illustrates how the isotherms change from mostly vertical behavior at low  $Ri$  to mostly horizontal behavior at high  $Ri$  which means dominated natural convection.

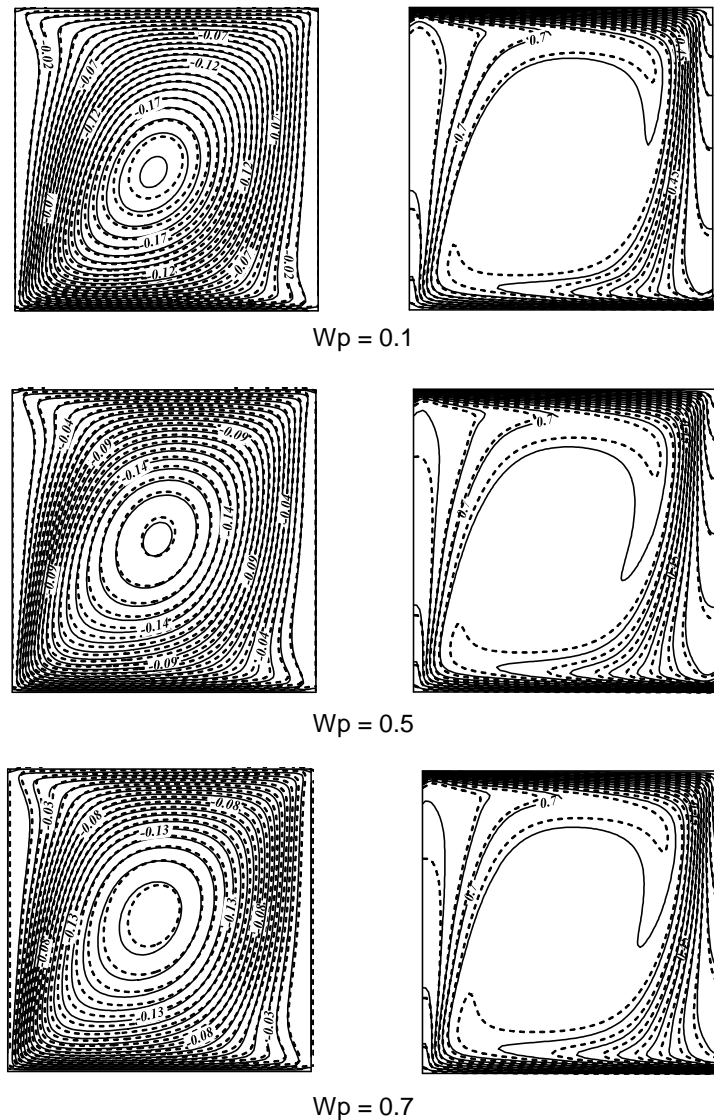


Fig. 4 Streamlines and isotherms for moving bottom and upper layers at different porous thickness layer at  $Ri = 1$ ,  $Da = 10^{-2}$ ,  $\phi = 0.0$  solid lines,  $\phi = 0.03$  dashed lines

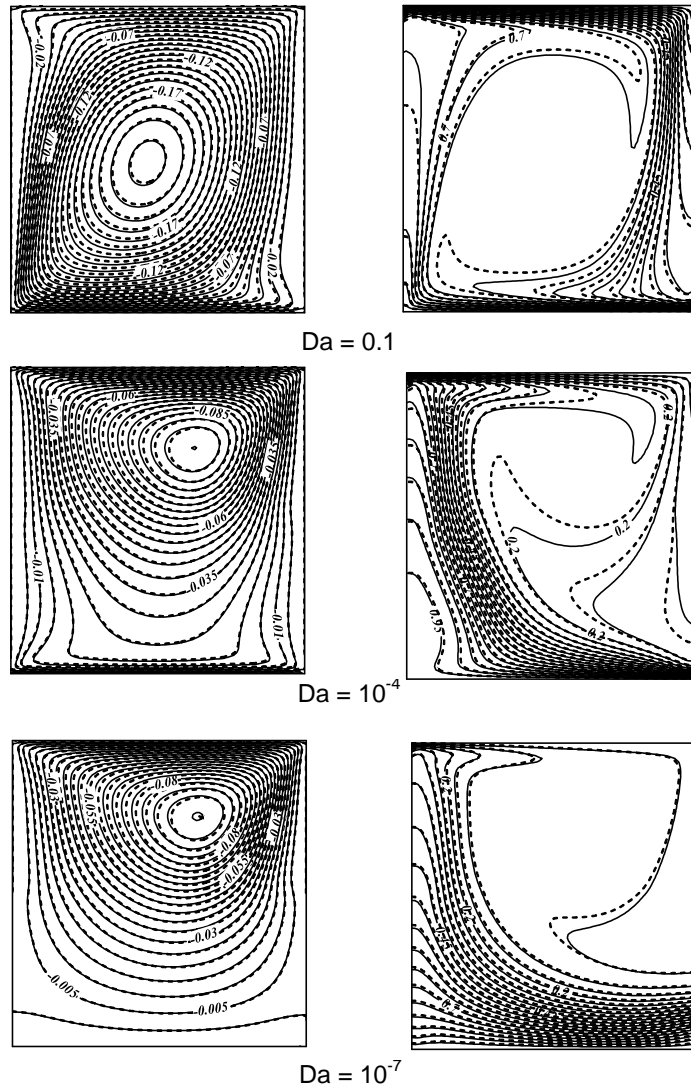


Fig. 5 Streamlines and isotherms for moving bottom and up layer at different Darcy number at  $Ri = 1$ ,  $Wp = 0.5$ ,  $\varphi = 0.0$  solid lines,  $\varphi = 0.03$  dashed lines

#### 4.2 Local and Average Nusselt Numbers

The distribution of the local Nusselt number  $Nu_{loc}$  along the moving bottom hot wall is presented in Figs. 7-9 for different parameters. Fig. 7 depicts the propagation of  $Nu_{loc}$  for  $Wp = 0.5$ ,  $Da = 10^{-5}$  and  $\varphi = 0.03$ . From this figure, no significant change observed when  $Ri$  increased from 0.01 to 0.1, however, the onset of  $Nu_{loc}$  variation is recorded at  $Ri \geq 1$ . This behavior is well expected because the forced convection is fixed in this study ( $Re = 100$ ), hence increasing  $Ri$  means increasing the natural convection only. The variations of  $Nu_{loc}$  for different porous layer thicknesses are depicted in Fig. 8. The like-peaks sudden changes in the  $Nu_{loc}$  refer to the perturbations indicated in the two ends of the moving bottom wall. The cause of these peaks (or perturbations) is attributed to the singularities resulting from meeting stationary and moving walls and also to that the fluid falling on the bottom wall will be suddenly driven by the shear friction resulting from the movement of the wall. The maximum values of  $Nu_{loc}$  are recorded at the mid of the

right half of the bottom wall. Figure 9 shows the distribution of  $Nu_{loc}$  along the bottom wall for different values of Darcy number while the other independent parameters are fixed at  $Ri = 10$ ,  $Wp = 0.7$  and  $\varphi = 0.05$ . It is clearly evidence that the effect of  $Da$  in this case is to be contrary with the other parameters. For  $Da < 10^{-3}$ , no noticeable variation is seen. For  $Da \geq 10^{-3}$ , Nusselt number increases along  $X$  with some peaks values close to the end of the moving wall. This behavior is mainly refers to the variation of the permeability of the porous layer

The average Nusselt number  $Nu_{av}$  over the moving bottom hot wall is presented in Figs. 10-16 for different independent parameters;  $Ri$ ,  $Da$ ,  $Wp$ , and  $\varphi$ . The effect of  $\varphi$  on the average Nusselt number for different porous layer thickness is shown in Fig. 10 for  $Ri = 1$ ,  $Da = 10^{-5}$ . The relatively low value of  $Da = 10^{-5}$  provides high resistance to flow which in turn makes the enhancement of heat transfer is very slight with increasing  $\varphi$  due to the existence of porous layer as it clearly evidence

where the slope of the curve referring to the lowest porous layer thickness ( $W_p = 0.1$ ) is greater than other  $W_p$  curves slopes. It is well known that when increasing the porous layer thickness, a corresponding reduction in  $Nu_{av}$  is obtained.

Figure 11 presents the variation of  $Nu_{av}$  with nanoparticles volume fraction for different values of  $Ri$ . It can be seen that the Richardson number has less effect in this case especially when  $Ri \leq 1$ . Figure 12 shows the effect of Darcy number for  $W_p = 0.9$  and  $Ri = 1.0$ . When  $Da > 10^{-5}$ ,  $Nu_{av}$  is rapidly increased to reach its maximum value at  $Da = 10^{-3}$ . In other words, this value of  $Da = 10^{-3}$  can be considered as a critical Darcy number. Figure 13 which is plotted for  $Ri = 0.1$ , also points out to that the maximum  $Nu_{av}$  is obtained at  $Da = 10^{-3}$  but for higher  $W_p$  values. Moreover, to inspect this critical value of  $Da$ , different examinations were made at different volume fractions and Richardson numbers as shown in Figs. 14 and 15, respectively. Figure 14 implies to an adverse action of nanoparticles when  $Da > 10^{-4}$ . This behavior can be attributed to the dominance effect of viscous and inertia forces associated with nanofluid over the thermal conductivity enhancement. However, examining Figs. 13-15, it can be emphasized that  $Da = 10^{-3}$  is a critical value when  $W_p > 0.5$ .  $Nu_{av}$  remains unchanged with increasing  $Da$  beyond  $10^{-3}$ .

The attribution of this phenomenon refers to that at larger values of  $W_p$  more drag within the porous layer exists and less penetration of streamlines occurs. When  $Da$  is increased, less drag and more penetration occurs, this will strengthen the momentum exchange between the two layers. When  $Da$  is further increased larger than  $Da = 10^{-3}$ , large amount of streamlines will penetrate through the porous layer which has low effective thermal conductivity (large heat resistance) and hence, an adverse action appears with increasing the permeability of the porous layer.

Figure 16 depicts the variation of the average Nusselt number with the porous layer thickness  $W_p$  for different values of Richardson number, at  $Da = 10^{-7}$  and  $\phi = 0.01$ . This figure demonstrates that the Richardson number is inactive when the porous layer thickness is approximately greater than 0.5, where when the whole cavity is porous medium, much drag to the natural convection is exerted. The most important result that can be drawn from this representation is that for dominant natural convection ( $Ri \gg 1$ ), the porous layer with a thickness value close to 0.3 can play a positive role in enhancing the convective heat transfer.

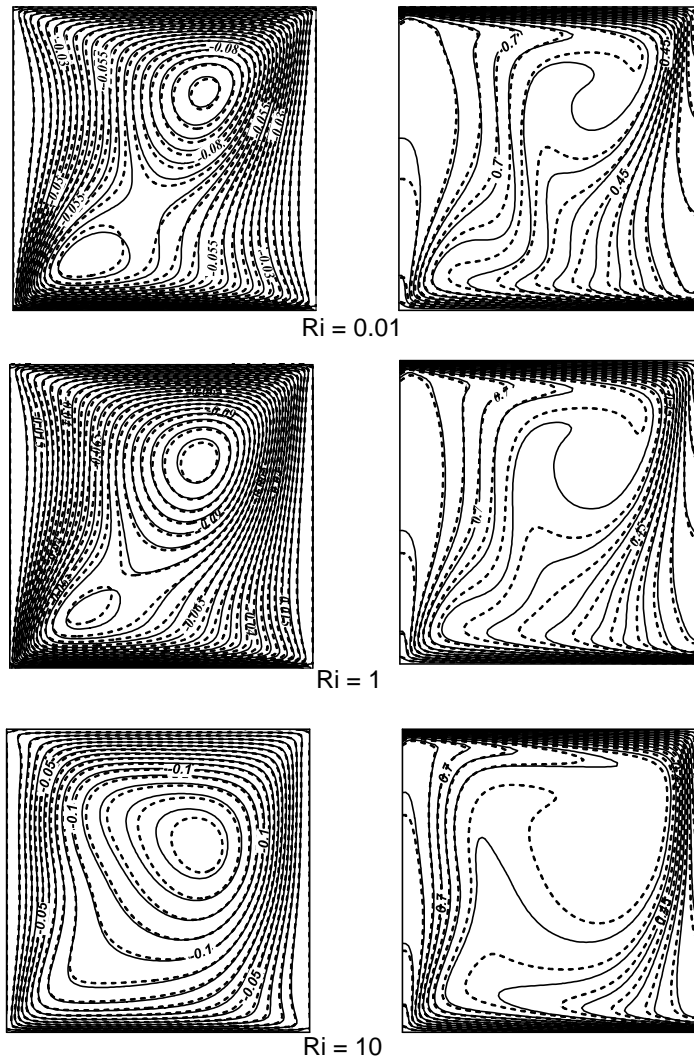


Fig. 6 Streamlines and isotherms for moving bottom and upper layers at different Richardson number at  $Da = 10^{-3}$ ,  $W_p = 0.5$ ,  $\phi = 0.03$  solid lines,  $\phi = 0.03$  dashed lines

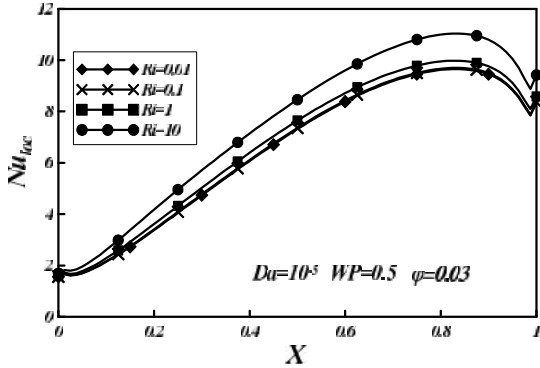


Fig. 7 Variation of the local Nusselt number along the bottom wall for different values of Richardson number

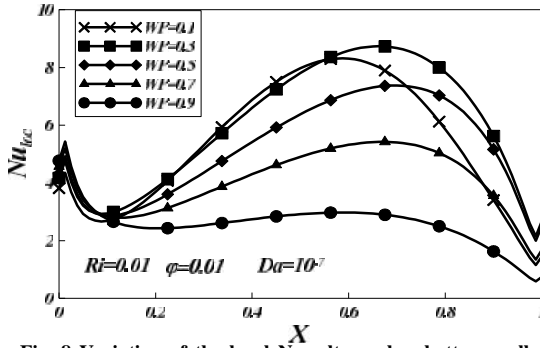


Fig. 8 Variation of the local Nusselt number bottom wall for different values of porous layer thickness

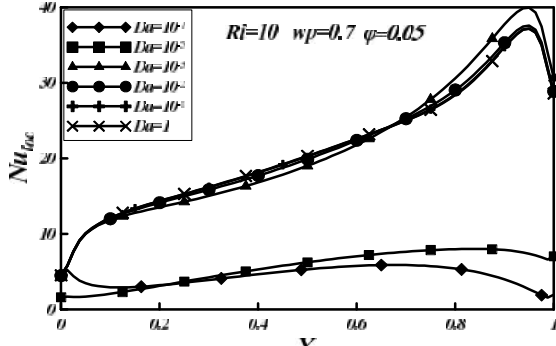


Fig. 9 Variation of the local Nusselt number along the bottom wall for different values of Darcy number

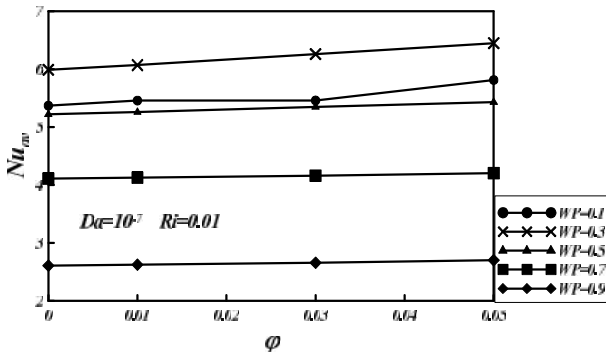


Fig. 10 Variation of the average Nusselt number with nanoparticles volume for different values of porous layer

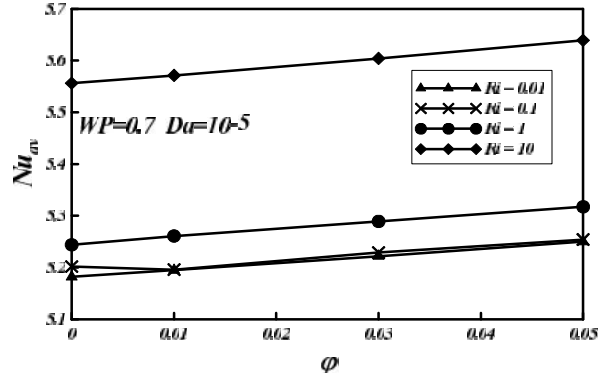


Fig. 11 Variation of the average Nusselt number with nanoparticles volume for different values of Richardson number

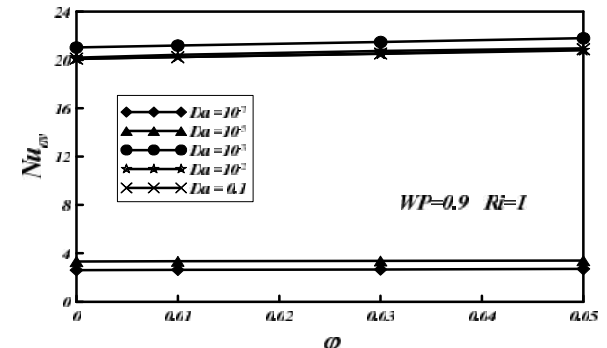


Fig. 12 Variation of the average Nusselt number with nanoparticles for different values of Darcy number

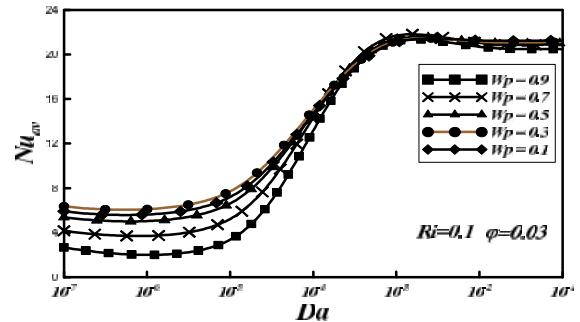


Fig. 13 Variation of the average Nusselt number with Darcy number for different values of porous layer thickness

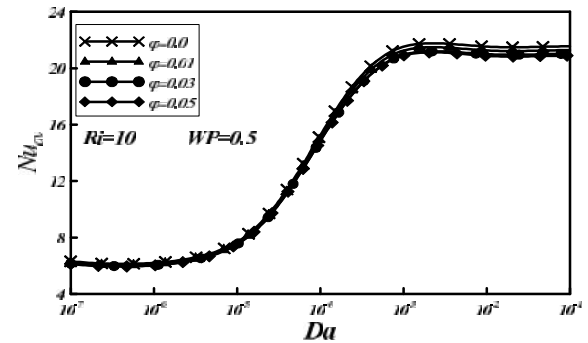


Fig. 14 Variation of the average Nusselt number with Darcy number for different values of nanoparticles volume fraction

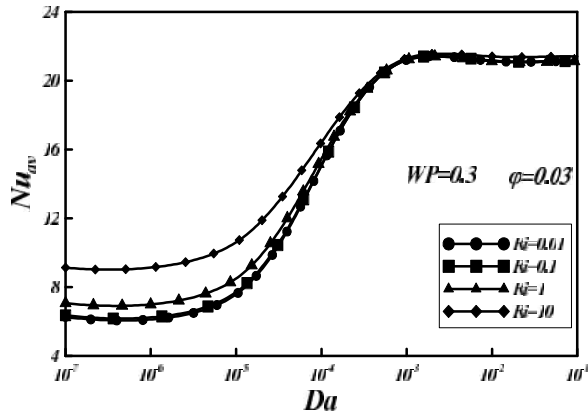


Fig. 15 Variation of the average Nusselt number with Darcy number for different values of Richardson number

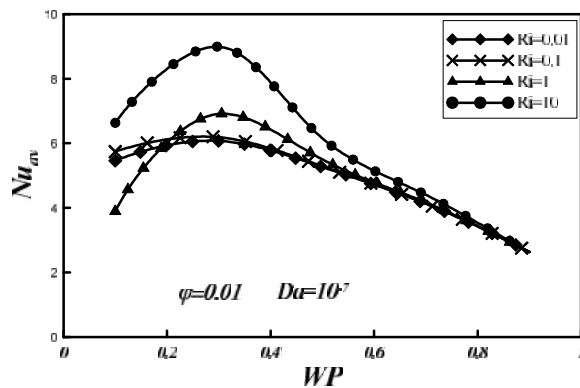


Fig. 16 Variation of the average Nusselt number with the porous layer thickness for different values of Richardson number

### 5. Conclusions

The present work investigates numerically the mixed convection inside a square lid-driven cavity composed of porous and nanofluid layers. The porous layer is saturated with the same nanofluid. Up-wind Finite Difference scheme was utilized in the numerical solution. Both horizontal walls are being lid. The primitive models of nanofluid properties were adopted, namely, Maxwell-Garante model for thermal conductivity and Brinkman model for dynamic viscosity. The numerical results have led to the following conclusions:

- 1- The value of  $Da = 10^{-3}$  can be considered as a critical value for  $Wp > 0.5$  where the average Nusselt number is maximum.
- 2- In general, the porous layer manifests an adverse role in enhancing the heat transfer inside the cavity. However, for dominant natural convection ( $Ri \geq 1$ ), the existence of porous layer with a thickness of about 0.3 plays a positive role in enhancing the convective heat transfer.
- 3- The strong mixing inside the cavity, due to the shear action, make the action of nanoparticles addition useless.
- 4- When the dimensionless permeability of the porous layer (Darcy number) is greater than  $10^{-4}$ , an adverse action of nanoparticles addition is observed.

### Nomenclature

$C_p$	Specific heat at constant pressure ( $J\ kg^{-1}\ K^{-1}$ )
$g$	Gravitational acceleration ( $m\ s^{-2}$ )
$Gr$	Grashof number, $Gr = g\ \rho_f (T_h - T_c) H^3 / \nu_f^2$
$H$	Height of the enclosure (m)
$k$	Thermal conductivity ( $W\ m^{-1}\ K^{-1}$ )
$K$	Permeability of the porous medium ( $m^2$ )
$Nu$	Nusselt number
$Pr$	Prandtl number, $Pr = \nu_f / \alpha_f$
$Re$	Reynolds number, $Re = U_o H / \nu_f$
$Ri$	Richardson number, $Ri = Gr / Re^2$
$T$	Temperature (K)
$u, v$	Velocity components ( $ms^{-1}$ )
$U, V$	Dimensionless velocities components
$U_o$	Lid velocity
$Wp$	Porous layer thickness (m)
$x, y$	Dimensional coordinates (m)
$X, Y$	Dimensionless coordinates, $X = x / H, Y = y / H$

### Greek symbols

$\alpha$	Thermal diffusivity ( $m^2\ s^{-1}$ )
$\beta$	Thermal expansion coefficient ( $K^{-1}$ )
$\epsilon$	porosity of the porous layer
$\phi$	Nanoparticle volume fraction
$\nu$	Kinematic viscosity ( $m^2\ S^{-1}$ )
$\theta$	Dimensionless temperature, $\theta = (T - T_c) / (T_h - T_c)$
$\psi$	Dimensional stream function ( $m^2\ S^{-1}$ )
$\Psi$	Dimensionless stream function, $\Psi = \psi / (U_o H)$
$\Omega$	Dimensional vorticity ( $S^{-1}$ )
$\Omega^*$	Dimensionless vorticity, $\Omega^* = \Omega / (U_o / H)$
$\rho$	Density ( $kg\ m^{-3}$ )
$\mu$	Dynamic viscosity ( $N.S\ m^{-2}$ )

### Subscript

av	Average
b	Bottom
c	Cold
f	Fluid
h	Hot
nf	Nanofluid
np	Nanoparticle
loc	Local
p	Porous
t	Top

### References

- [1] K. Torrance, R. Davis, K. Eike, P. Gill, D. Gutman, A. Hsui, S. Lyons, H. Zien, Cavity flows driven by buoyancy and shear, J. Fluid Mech. 1972; 51: 221–231, [Doi.org/10.1017/S0022112072001181](https://doi.org/10.1017/S0022112072001181)
- [2] U. Ghia, K.N. Ghia, C.T. Shin, High-Re solutions for incompressible flow using the Navier–Stokes equations and a multigrid method, J. of Computational Physics 1982; 48: 367-411, [Doi.org/10.1016/0021-9991\(82\)90058-4](https://doi.org/10.1016/0021-9991(82)90058-4)

- [3] J.R. Koseff, R.L. Street, The Lid-Driven Cavity Flow: A Synthesis of Qualitative and Quantitative Observations, *J. Fluids Eng.* 1984; 106: 390-398, [Doi:10.1115/1.3243136](https://doi.org/10.1115/1.3243136)
- [4] A.A. Mohamad and R. Viskanta, Flow and thermal structures in a lid-driven cavity heated from below, *Fluid Dynamics Research* 1993;12: 173-184, [Doi.org/10.1016/0169-5983\(93\)90021-2](https://doi.org/10.1016/0169-5983(93)90021-2)
- [5] S. Mekroussi, D. Nehari, M. Bouzit, N.S. Chemloul, Analysis of mixed convection in an inclined lid-driven cavity with a wavy wall, *J. of Mechanical Science and Technology* 2013; 27: 2181-2190, [Doi :10.1007/s12206-013-0533-9](https://doi.org/10.1007/s12206-013-0533-9)
- [6] S. Sivasankaran, V. Sivakumar, A.K. Hussein, Numerical study on mixed convection in an inclined lid-driven cavity with discrete heating, *Int. Communications in Heat and Mass Transfer* 2013; 46:112125, [Doi.org/10.1016/j.icheatmasstransfer.2013.05.022](https://doi.org/10.1016/j.icheatmasstransfer.2013.05.022)
- [7] R.K. Tiwari, M.K. Das, Heat transfer augmentation in a two-sided lid-driven differentially heated square cavity utilizing nanofluids, *Int. J. of Heat and Mass Transfer* 2007; 50: 2002–2018, [Doi.org/10.1016/j.ijheatmasstransfer.2006.09.034](https://doi.org/10.1016/j.ijheatmasstransfer.2006.09.034)
- [8] F. Talebi, A.H. Mahmoudi, M. Shahi, Numerical study of mixed convection flows in a square lid-driven cavity utilizing nanofluid, *Int. Communications in Heat and Mass Transfer* 2010; 37:79–90. [Doi.org/10.1016/j.icheatmasstransfer.2009.08.013](https://doi.org/10.1016/j.icheatmasstransfer.2009.08.013)
- [9] E. Abu-Nada, A.J. Chamkha, Mixed convection flow in a lid-driven inclined square enclosure filled with a nanofluid, *European J. of Mechanics B/Fluids*, 2010; 29: 472-482. [Doi.org/10.1016/j.euromechflu.2010.06.008](https://doi.org/10.1016/j.euromechflu.2010.06.008)
- [10] A.J. Chamkha, E. Abu-Nada, Mixed convection flow in single- and double-lid driven square cavities filled with water–Al<sub>2</sub>O<sub>3</sub> nanofluid: Effect of viscosity models, *European J. of Mechanics B/Fluids* 2012; 36: 82–96, [Doi.org/10.1016/j.euromechflu.2012.03.005](https://doi.org/10.1016/j.euromechflu.2012.03.005)
- [11] A.A. Abbasian Arani, S.M. Sebdani, M. Mahmoodi, A. Ardeshiri , M. Aliakbari, Numerical study of mixed convection flow in a lid-driven cavity with sinusoidal heating on sidewalls using nanofluid, *Superlattices and Microstructures* 2012; 51: 893–911, [Doi.org/10.1016/j.spmi.2012.02.015](https://doi.org/10.1016/j.spmi.2012.02.015)
- [12] Ching-Chang Cho, Chieh-Li Chen, Cha'o-Kuang Chen, Mixed convection heat transfer performance of water-based nanofluids in lid-driven cavity with wavy surfaces, *Int. J. of Thermal Sciences* 2013; 68: 181-190, [Doi.org/10.1016/j.ijthermalsci.2013.01.013](https://doi.org/10.1016/j.ijthermalsci.2013.01.013)
- [13] H.F. Oztop, Combined convection heat transfer in a porous lid-driven enclosure due to heater with finite length, *Int. communications in heat and mass transfer* 2006; 33: 772-779, [Doi.org/10.1016/j.icheatmasstransfer.2006.02.003](https://doi.org/10.1016/j.icheatmasstransfer.2006.02.003)
- [14] M. Muthamilselvan, P. Kandaswamy, and J. Lee, Hydromagnetic mixed convection in a lid-driven cavity filled with a fluid-saturated porous medium, *Int. J. of Appl. Math. and Mech.* 2009; 5: 28-44, [Doi: 10.1615/InterJFluidMechRes.v37.i5.20](https://doi.org/10.1615/InterJFluidMechRes.v37.i5.20)
- [15] Q. Sun, I. Pop, Free convection in a triangle cavity filled with a porous medium saturated with nanofluids with flush mounted heater on the wall, *Int. J. of Thermal Sciences* 2011; 50: 2141-2153, [Doi.org/10.1016/j.ijthermalsci.2011.06.005](https://doi.org/10.1016/j.ijthermalsci.2011.06.005)
- [16] A.J. Chamkha, M. A. Ismael, Conjugate heat transfer in a porous cavity filled with nanofluids and heated by a triangular thick wall, *Int. J. of Thermal Sciences* 2013; 67: 135-151, [Doi.org/10.1016/j.ijthermalsci.2012.12.002](https://doi.org/10.1016/j.ijthermalsci.2012.12.002)
- [17] G.C. Bourantas, E.D. Skouras, V.C. Loukopoulos, V.N. Burganos, Heat transfer and natural convection of nanofluids in porous media, *European J. of Mechanics B/Fluids* 2014; 43: 45–56, [Doi.org/10.1016/j.euromechflu.2013.06.013](https://doi.org/10.1016/j.euromechflu.2013.06.013)
- [18] M.H.M Yasin, N.M. Arifin, R. Nazar, F. Ismail, I. pop, Mixed convection boundary layer flow on a vertical surface in a porous medium saturated by a nanofluid with suction or injection. *J. of Mathematics and Statistics* 2013; 9: 119-128,
- [19] F. Chen, C.F. Chen, Convection in superposed fluid and porous layers, *J. of Fluid Mech.* 1992: 234: 97-119, [Doi: 10.1017/S0022112092000727](https://doi.org/10.1017/S0022112092000727)
- [20] B. Goyeau, D. Lhuillier, D. Gobin, M.G. Velarde, Momentum transport at a fluid–porous interface, *Int. J. of Heat and Mass Transfer* 2003; 234: 4071–408, [Doi.org/10.1016/S0017-9310\(03\)00241-2](https://doi.org/10.1016/S0017-9310(03)00241-2)
- [21] A.C. Baytas, A.F. Baytas, D.B. Ingham, I. Pop, Double diffusive natural convection in an enclosure filled with a step type porous layer: Non-Darcy flow, *Int. J. of Thermal Sciences* 2009; 48: 665–673, [Doi.org/10.1016/j.ijthermalsci.2008.06.001](https://doi.org/10.1016/j.ijthermalsci.2008.06.001)
- [22] A. Bagchi, F.A. Kulacki , Natural convection in fluid–superposed porous layers heated locally from below, *Int. J. of Heat and Mass Transfer* 2011; 54: 3672–3682, [Doi.org/10.1016/j.ijheatmasstransfer.2011.01.034](https://doi.org/10.1016/j.ijheatmasstransfer.2011.01.034)
- [23] A. Bagchi, F.A. Kulacki, Experimental study of natural convection in fluid-superposed porous layers heated locally from below, *Int. J. of Heat and Mass Transfer* 2012; 55: 1149–1153, [Doi.org/10.1016/j.ijheatmasstransfer.2011.09.056](https://doi.org/10.1016/j.ijheatmasstransfer.2011.09.056)
- [24] A.J. Chamkha, M.A. Ismael, Natural convection in differentially heated partially porous layered cavities filled with nanofluid, *Numerical Heat Transfer Part A*, 2014; 65: 1089-1113, [Doi: 10.1080/10407782.2013.851560](https://doi.org/10.1080/10407782.2013.851560)

- [25] H.C. Brinkman, The viscosity of concentrated suspensions and solutions, *J. Chem. Phys.* 1952; 20: 571, [Doi.org/10.1063/1.1700493](https://doi.org/10.1063/1.1700493)
- [26] K. Khanafer, K. Vafai, M. Lightstone, Buoyancy-driven heat transfer enhancement in a two-dimensional enclosure utilizing nanofluids, *Int. J. Heat Mass Transfer* 2003; 46: 3639-3653, [Doi.org/10.1016/S0017-9310\(03\)00156-X](https://doi.org/10.1016/S0017-9310(03)00156-X)
- [27] G. Neale, W. Nader, Practical significance of Brinkman's extension of Darcy's law: coupled parallel flows within a channel and a bounding porous medium, *Can. J. Chem. Eng.* 1974; 52: 475–478, [Doi:10.1002/cjce.5450520407](https://doi.org/10.1002/cjce.5450520407)
- [28] M.A. Sheremet, T.A. Trifonova, Unsteady conjugate natural convection in a vertical cylinder containing a horizontal porous layer: Darcy model and Brinkman-extended Darcy model, *Transp Porous Med.* 2014; 101: 437–463. [Doi: 10.1007/s11242-013-0253-8](https://doi.org/10.1007/s11242-013-0253-8)
- [29] E. Weinan, Liu J.-G., Vorticity boundary condition and related issues for finite difference schemes, *J. Comput. Phys.* 1996; 124: 368–382, [Doi.org/10.1006/jcph.1996.0066](https://doi.org/10.1006/jcph.1996.0066)
- [30] M.A. Waheed, Mixed convective heat transfer in rectangular enclosures driven by a continuously moving horizontal plate, *Int. J. Heat Mass Transfer* 2009; 52: 5055-5063, [Doi.org/10.1016/j.ijheatmasstransfer.2009.05.011](https://doi.org/10.1016/j.ijheatmasstransfer.2009.05.011)